TURBULENCE AND LARGE-EDDY SIMULATIONS

Marcel R. Lesieur
Geophysical and Industrial Flows Lab. (LEGI)
BP 53, 38041 Grenoble-Cedex 9. France
marcel.lesieur@inpg.fr

Abstract After having discussed the limits of turbulence direct-numerical simulations, one presents large-eddy simulations methods, where small scales are filtered out and modelled by appropriate eddy coefficients in the evolution of large scales. We concentrate on models developed originally in Fourier space, then adapted to physical space. One presents coherent-vortex dynamics and statistical data obtained thanks to these models for incompressible isotropic turbulence, channel flow and controlled round jet. Then large-eddy simulations are considered in the compressible case, where we study first the free jet at Mach 0.7 and 1.4, then the controlled supersonic jet. Finally LES of compressible flows above riblets in subsonic and supersonic cases are considered.

Keywords: Turbulence, large-eddy simulations, coherent vortices, jets, compressible flows, control, riblets.

Introduction

Direct-numerical simulations (DNS) of turbulence are based on deterministic solutions of Navier-Stokes equation, obtained through a proper discretization on a spatio-temporal grid of partial-differential operators involved, and where one advances in time starting from a given initial state. This implies that the typical grid mesh Δx in space should be inferior to the Kolmogorov scale $l_D = k_D^{-1}$, under which velocity fluctuations are damped out by molecular viscosity. Another important point is that numerical schemes should be sufficiently precise, and hence of high order, if possible. In fact the number of spatial grid points necessary for a well-resolved DNS in developed three-dimensional turbulence is $\approx (L/l_D)^3$, where L is the typical size of large structures. One can show that this is of the order of $\sim R_\lambda^{9/2}$, where $R_\lambda = u'\lambda/\nu$ is defined thanks to the rms longitudinal velocity and the Taylor microscale. R_λ may

be determined experimentally, for instance on a commercial-plane wing where it is equal to 3000 (Jimenez, 2000). This yields $\approx 10^{15}$ grid points to handle on the computer, which permits to envisage a DNS of such a flow within 30 to 50 years. For the atmospheric boundary layer it is worse, since we have $R_\lambda = 10000$, and hence 10^{18} grid points. To be able to perform a simulation in such cases, one is thus obliged to reduce drastically the number of degrees of freedom of the system. Large-eddy simulations (LES) are a powerful tool for this purpose. More details concerning the rest of this talk may be found in Lesieur (1997), Lesieur & Métais (1996), and Lesieur et al. (2004).

1. Incompressible LES

Physical Space

Density $\rho = \rho_0$ is uniform. Let Δx be a given spatial grid mesh comprised between L and l_D, and $G_{\Delta x}$ a low-pass spatial filter of width Δx, chosen in order to eliminate properly subgridscale motions of wavelength $< \Delta x$. One associates to any quantity $f(\vec{x}, t)$ its locally-filtered counterpart

$$\bar{f}(\vec{x}, t) = f * G_{\Delta x} = \int f(\vec{y}, t) G_{\Delta x}(\vec{x} - \vec{y}) d\vec{y}. \tag{1}$$

The filter commutes with spatial and temporal derivatives (if Δx is uniform). Let us write Navier-Stokes equation as

$$\frac{\partial u_i}{\partial t} + \frac{\partial}{\partial x_j}(u_i u_j) = -\frac{1}{\rho_0}\ \frac{\partial p}{\partial x_i} + \frac{\partial}{\partial x_j}(2\nu S_{ij}), \tag{2}$$

where

$$S_{ij} = \frac{1}{2}\left(\frac{\partial u_i}{\partial x_j} + \frac{\partial u_j}{\partial x_i}\right) \tag{3}$$

is the deformation tensor, symmetric part of the velocity gradient, and ν is assumed constant. When applying the filter, it is obtained

$$\frac{\partial \bar{u}_i}{\partial t} + \frac{\partial}{\partial x_j}(\bar{u}_i \bar{u}_j) = -\frac{1}{\rho_0}\ \frac{\partial \bar{p}}{\partial x_i} + \frac{\partial}{\partial x_j}(2\nu \bar{S}_{ij} + \bar{u}_i \bar{u}_j - \overline{u_i u_j}). \tag{4}$$

I call $T_{ij} = \bar{u}_i \bar{u}_j - \overline{u_i u_j}$ the subgrid-stresses tensor. This is in fact Navier-Stokes equation for $\bar{u}_i$, provided T_{ij} is added to the filtered viscous stress $2\nu \bar{S}_{ij}$. Continuity $\partial \bar{u}_j / \partial x_j = 0$ holds for the filtered Navier-Stokes equation if Δx is uniform. The simplest way chosen to close the problem is to make an eddy-viscosity assumption

$$T_{ij} = 2\nu_t(\vec{x}, t)\ \bar{S}_{ij} + \frac{1}{3} T_{ll}\ \delta_{ij}, \tag{5}$$

where ν_t has to be determined (see later). With such an hypothesis, the filtered Navier-Stokes equation writes

$$\frac{\partial \bar{u}_i}{\partial t} + \frac{\partial}{\partial x_j}(\bar{u}_i \bar{u}_j) = -\frac{1}{\rho_0}\frac{\partial \bar{P}}{\partial x_i} + \frac{\partial}{\partial x_j}[2(\nu + \nu_t)\bar{S}_{ij}], \tag{6}$$

where one has introduced a modified pressure (macro-pressure)

$$\bar{P} = \bar{p} - \frac{1}{3}\rho_0 T_{ll}. \tag{7}$$

Let us now consider the mixing of a scalar $T(\vec{x}, t)$ transported by the flow (with a molecular diffusivity κ), which obeys heat Fourier equation following the fluid motion:

$$\frac{\partial T}{dt} + \frac{\partial}{\partial x_j}(T\ u_j) = \frac{\partial}{\partial x_j}\left\{\kappa \frac{\partial T}{\partial x_j}\right\}\ . \tag{8}$$

Filtering this equation and making the assumption of an eddy diffusivity $\kappa_t(\vec{x}, t)$ yields for the filtered scalar:

$$\frac{\partial \bar{T}}{dt} + \frac{\partial}{\partial x_j}(\bar{T}\ \bar{u}_j) = \frac{\partial}{\partial x_j}\left\{(\kappa + \kappa_t)\frac{\partial \bar{T}}{\partial x_j}\right\}\ . \tag{9}$$

$\kappa_t(\vec{x}, t)$ is determined from ν_t thanks to a "turbulent Prandtl number" $P_r^{(t)} = \nu_t/\kappa_t$. These eddy coefficients need to be determined. In Smagorinsky's model (1963), the eddy viscosity is based on velocity gradients and taken proportional to $(\Delta x)^2\sqrt{\bar{S}_{ij}\bar{S}_{ij}}$. There are interesting improvements of this model made by Germano et al. (1991) where the constant is calculated dynamically by a double filtering. In fact, the major drawback of an eddy-viscosity assumption in physical space is that it assumes a scale-separation between filtered and subgridscales, as the molecular-viscosity concept in a continuous medium is based upon the existence of a scale separation between macroscopic and molecular scales. This explains the poor correlation between T_{ij} and $\bar{S}_{ij}$ found in a-priori tests based on DNS. This is a serious motivation to work in Fourier space if the geometry of the problem permits it.

Grenoble Models in Fourier Space

Turbulence is first assumed statistically homogeneous. Let $\hat{f}(\vec{k}, t)$ be the spatial Fourier transform of any quantity $f(\vec{x}, t)$:

$$\hat{f}(\vec{k}, t) = \left(\frac{1}{2\pi}\right)^3 \int e^{-i\vec{k}.\vec{x}} f(\vec{x}, t)\ d\vec{x}. \tag{10}$$

The optimal filter to eliminate small scales considered as waves with a given spatial wavelength is a sharp filter, such that

$$\overline{\hat{f}} = \hat{f} \quad \text{for} \quad k = |\vec{k}| < k_C = \frac{\pi}{\Delta x} \; ; \; \overline{\hat{f}} = 0 \quad \text{for} \quad k > k_C \; , \tag{11}$$

the factor $\pi/\Delta x$ coming when one works using pseudo-spectral methods in a spatially-periodic flow. If turbulence is statistically isotropic, one can define the kinetic-energy spectrum $E(k,t)$, such that $E(k,t)\delta k$ is the mean (in the sense of a statistical average upon an ensemble of realizations) kinetic energy per unit mass in a spatial-frequency band $[k, k+\delta k]$.

In Fourier space, nonlinear interactions go through "resonant" triads of wavevectors such that $\vec{k} = \vec{p} + \vec{q}$. Indeed, due to incompressibility, the nonlinear term of Navier-Stokes turns out to be the projection in a plane perpendicular to $\vec{k}$ of the Fourier transform of $(\partial/\partial x_j)u_i u_j$, equal to k_j times the Fourier transform of $u_i u_j$, which is a convolution product in Fourier space (Remark that the so-called "projection methods" in the numerical analysis of Navier-Stokes equation are based on that). The subgrid modelling consists here in evaluting the momentum transfers due to triads where $k < k_C$ and one at least of wavenumbers p and q is larger than k_C. In analogy with the fact that the Fourier transform of Navier-Stokes dissipative term is $-\nu k^2 \hat{u}_i(\vec{k},t)$, the subgrid momentum transfer will be modelled as $-\nu_t(k|k_C)k^2\hat{u}_i(\vec{k},t)$, the eddy viscosity in spectral space being calculated at the level of subgrid kinetic-energy transfers through an advanced theory of turbulence, the EDQNM. One gets

$$\nu_t(k|k_C) = 0.441 {C_K}^{-3/2} \left[\frac{E(k_C)}{k_C}\right]^{1/2} X\left(\frac{k}{k_C}\right), \tag{12}$$

assuming that k_C lies in a Kolmogorov spectrum $E(k) = C_K \epsilon^{2/3} k^{-5/3}$. Here, $X(k/k_C)$ is a "plateau-peak function" equal to 1 for $k/k_C <\approx 1/3$, and rising above. In fact, ν_t^+ on Fig. 1 is the spectral eddy viscosity renormalized by $\sqrt{E(k_C)/k_C}$. Notice that the same kind of eddy-viscosity had been found by Kraichnan (1976) with another turbulence stochastic model, the Test-Field model, but he did not consider the scaling in $\sqrt{E(k_C)/k_C}$, nor used this spectral eddy-viscosity for LES purposes. Figure 1 shows also the renormalized eddy-diffusivity, which has the same scaling and plateau-peak behaviour, and the turbulent Prandtl number, approximately constant and equal to 0.6. This plateau-peak model has been used by Chollet & Lesieur (1981) to perform the first LES of three-dimensional isotropic turbulence. In fact, it was shown numerically by Domaradzki et al. (1987) on the basis of direct-numerical

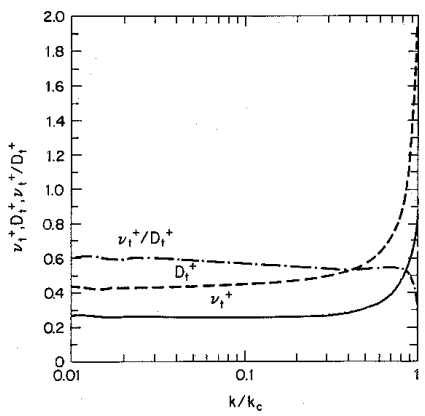

Figure 1. Spectral eddy viscosity, diffusivity and turbulent Prandtl number calculated using the EDQNM theory (from Chollet & Lesieur, 1981)

simulations that the plateau part of the eddy viscosity goes to 0 at low Reynolds number. In the spectral-dynamic model (Lamballais, Métais and Lesieur, 1998), one accounts (still thanks to the EDQNM theory) in the plateau elevation for a spectral slope at k_C different from 5/3.

We give two applications of this model: the first one concerns the decay of isotropic turbulence at zero molecular viscosity in a periodic box, starting from a Gaussian velocity profile. Pseudo-spectral numerical methods are used. The initial peak is $k_i = 4$. One presents an animation taken from Lesieur et al. (2003, 2004) showing the formation and evolution of the spaghetti-type vortices. They are identified thanks to isosurfaces at a positive fixed threshold of $Q = (1/2)(\Omega_{ij}\Omega_{ij} - S_{ij}S_{ij})$, the second invariant of the velocity gradient. This criterion, due to Hunt et al. (1988), characterizes regions where local rotation dominates deformation, and where pressure has a local minimum. This criterion is very efficient to visualize coherent vortices, and simpler to implement than its very close cousin the λ_2 criterion of Jeong & Hussain (1995).

The spectral-dynamic model has also been applied to a plane channel of width $2h$ at $h^+ = 204$ and 395. The symbol $^+$ means that length is normalized by the viscous length ν/v_*, which is equivalent for a boundary layer to Kolmogorov dissipative scale. Numerical methods are here pseudo-spectral in directions parallel to the walls, and finite differences of sixth order in the normal direction. A calculation with the first grid point at a distance of one viscous length from the wall (and a stretched grid away) yields very good statistical results compared with Kim's DNS published in Antonia et al. (1992). At $h^+ = 395$, the LES is 70 times faster than the DNS.

It is clear that the use of stretched grids invalidates the assumption of regular grid done above. However, LES carried out in this improper manner give valuable results concerning statistics and coherent-vortex dynamics, as far as comparisons with experiments and DNS are done.

Grenoble Models in Physical Space: Structure-function Models

For complicated geometries, numerical methods impose to work in physical space. The spectral eddy viscosity is thus set to a constant calculated assuming the subgrid kinetic-energy dissipation equals ϵ in a Kolmogorov cascade. Then we lose the advantage of not assuming a spectral gap. But results of the model are however good, as it will be seen. We have $\nu_t(\vec{x}, \Delta x) = (2/3)C_K^{-3/2} \left[E_{\vec{x}}(k_C)/k_C)\right]^{1/2}$, where $E_{\vec{x}}(k_C)$ is a local kinetic-energy spectrum, determined with the aid of the local second-order velocity structure function. This model, due to Métais & Lesieur (1992), improves classical Smagorinsky model for non-sheared turbulence. For sheared turbulence (without or with walls), two excellent versions of the model exist to eliminate the damping effects of large-scale shears: the selective structure-function model (David, 1993), and the filtered structure-function model (Ducros et al., 1996). They work very well for free-shear flows and boundary layers and can be utilized on unstructured grids.

An example is provided with the control by upstream perturbations (superposed to a close to top hat profile) of a round jet, presented in Silva & Métais (2003). The calculation involves the combination of "harmonic varicose" and "sub-harmonic flapping" modes (harmonic is defined with respect to the preferred frequency of vortices shed in the free jet and passing at the level of the potential core). In such a flow, the jet collapses in the so-called bisecting plane, and widens in the bifurcating plane. It is possible to see on an animation (enclosed on the CD-ROM) of positive Q isosurfaces in a LES at molecular Reynolds number 5000. The numerical code is the same as for the channel presented above, with a Cartesian orthogonal system of coordinates. Resolution is $201 \times 128 \times 128$. In the animation, the jet is artificially rotating from the bisecting to the bifurcating planes. One can see in particular alternate-pairing interaction between vortex rings, which is a sub-harmonic reconnection of vortices, analogous to helical pairing of Kelvin-Helmholtz vortices found in DNS and LES of temporal mixing layers (see eg Comte et al., 1992). With other types of forcings, one can generate Reynolds blooming jet.

2. Compressible LES

Formalism

We work with an ideal gas. The LES formalism is much more complicated in the compressible case. Equations expressing conservation of mass, total momentum $\rho\vec{u}$ and total energy ρe are still filtered by the "bar-filter". Gravity is neglected. One can make important simplifications by using Favre filtering $\tilde{f}$ and introducing a "macro-temperature"

$$\vartheta = \widetilde{T} - \frac{\mathcal{T}_{ll}}{2C_v\overline{\rho}} \quad , \tag{13}$$

where $\mathcal{T}_{ll}$ is the trace of the subgridscale tensor $\mathcal{T}_{ij} = \overline{\rho}\tilde{u}_i\tilde{u}_j - \overline{\rho u_i u_j}$. The latter is related to the macro-pressure ϖ by the relation

$$\varpi = \overline{\rho}R\vartheta + \frac{3\gamma - 5}{6}\mathcal{T}_{ll} \quad . \tag{14}$$

In this relation, the last term is small even at high Mach, so that we neglect it and use the law of ideal gases between $\varpi, \overline{\rho}$ and ϑ. After some other approximations, one obtains a system equivalent to compressible Navier-Stokes equation for $\widetilde{u_i}, \bar{\rho}, \varpi, \vartheta, \widetilde{e}$, most of the molecular-diffusion coefficients being complemented by an eddy counterpart which is the same as in the incompressible case. We work with the filtered structure-function model.

Round Jet

Then one studies a compressible round jet at Mach (defined at the upstream jet centreline) 0.7 and 1.4 forced upstream by a close to top-hat velocity to which a weak isotropic random perturbation is superposed. The associated temperature profile is given by Crocco-Busemann relation for a boundary-layer without pressure-gradient.

Numerical methods are now for nonlinear terms fourth-order MacCormack's predictor-corrector scheme modified by Gottlieb & Turkel (1976). Boundary conditions are based upon Poinsot & Lele (1992) characteristics-based method, with a sponge zone downstream, following the procedure developed by Sandhu and Sandham (1994). The Reynolds number is 36000. We show on Fig. 2 a picture of the jet (top, Mach 0.7; bottom Mach 1.4) in the case of a white-noise forcing: the supersonic jet is much more focussed in space than the subsonic one, with an increase of the potential core. This is related to the delay of Kelvin-Helmholtz instability due to convective Mach number effects, as shown by Papamoschou & and Roshko (1988) in an experimental spatially-growing mixing layer, and by Sandham & Reynolds (1991) for temporal mixing layers. Further

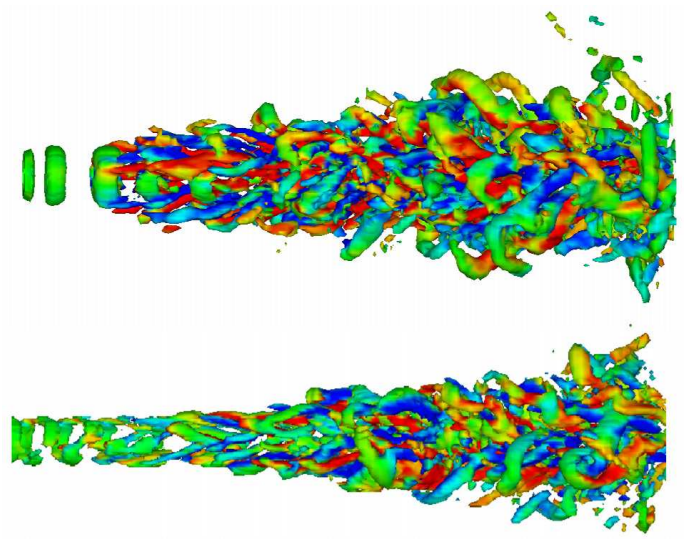

Figure 2. LES of a compressible round jet forced by a weak isotropic random perturbation. Positive Q isosurfaces coloured by longitudinal vorticity. Top, Mach 0.7; bottom, Mach 1.4 (courtesy M. Maidi).

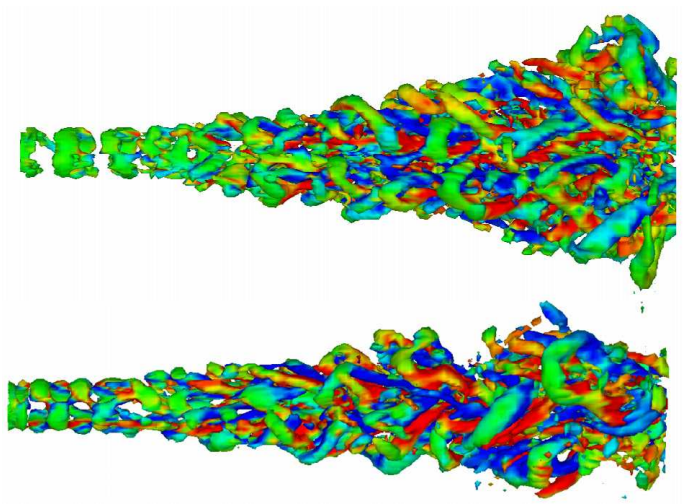

Figure 3. LES of a the forced jet at Mach 1.4. Positive Q isosurfaces coloured by longitudinal vorticity. Top, bifurcating plane; bottom, bisecting plane (courtesy M. Maidi).

downstream, the supersonic jet has reduced its convective Mach number, and starts spreading out as the subsonic one. Notice that the supersonic jet we have simulated does not exit from a real nozzle, and no shocks or Mach waves can be produced. We have estimated the noise radiated away from the jets on the basis of an approximate Lighthill equation due to Witkowska and Juve (1994), and found that the supersonic jet is much more noisy than the subsonic one. This agrees with laws predicting that the acoustic energy is proportional to the jet exit velocity raised to a high power.

Let us now consider the LES of a jet at Mach 1.4 and Reynolds 36000 controlled by the same mixed harmonic varicose/sub-harmonic flapping upstream perturbation as in the incompressible case. Figure 3 presents Q coloured by longitudinal vorticity in the bifurcating and bisecting planes.

Drag Reduction by Riblets

We briefly recall the numerous studies associated to passive turbulence control by longitudinal riblets put on some parts of planes, boats, and more recently on competition swimming costumes made of so-called shark skin. The optimal spanwise wavelength of triangular riblets was empirically found to be $\lambda_z^+ = 10 \approx 20$. In fact, the DNS of Choi et al. (1993) using equilateral triangles have shed a new light on the role of quasi-longitudinal vortices in drag reduction by riblets. Indeed, the diameter of quasi-longitudinal vortices travelling in a turbulent boundary layer on a flat plate is $d^+ \approx 25$. Choi et al's DNS show that for λ_z^+ larger than 25 (they took 40), the quasi-longitudinal vortices are trapped in the valleys of the riblets, which increases the drag. On the other hand, in the simulation with $\lambda_z^+ = 20$, the longitudinal vortices sit above the riblets peak, and the drag is decreased.

A very important question for aeronautic applications concerns the influence of compressibility in a perfect gas for riblets efficiency. For this purpose, we consider a compressible channel of ideal gas, one wall being flat and the other equipped of longitudinal triangular riblets. Our LES are the continuation of compressible-channel DNS (with two flat walls) of Coleman et al. (1995) and Lechner et al. (2001). One defines the bulk density ρ_b and velocity U_b as

$$2h\rho_b = \int_{-h}^{+h} \langle\rho\rangle dy, \quad 2h\rho_b U_b = \int_{-h}^{+h} \langle\rho u\rangle dy. \tag{15}$$

Simulations are carried out at fixed bulk density and wall temperature T_w, whatever the Mach number. The latter is defined as U_b/c_w, c_w being the sound speed at the wall. The Reynolds number is $\rho_b U_b h/\mu_w$, in which

μ_w is the dynamic viscosity at the wall. For each U_b, the simulation is thus done at constant mass flux, which generates a turbulent state rapidly. The velocity gradients within the channel produce a heating by molecular-viscous effects, and the channel interior becomes warmer than the walls. Coleman et al. (1995) and Lechner et al. (2001) show that, when turbulence has developed, the average temperature (resp. density) remain approximately uniform in the major part of the channel, while decreasing (resp. rising) close to the walls. The inner plateau-part of the density is very slightly inferior to ρ_b.

LES of the same problem using the selective-structure function model and well-validated immersed-boundary methods have been carried out in Grenoble by Hauët (2003). Hauët has also developed LES at Reynolds 6000 of the compressible channel, one side of which is equipped of longitudinal triangular riblets. Two riblets were studied: the "high" one, of height and width (at Mach 0.33) 11 and 22 wall units; the "great" one, of height and width (at Mach 0.33) 22 and 44 wall units. Hauët has first validated satisfactorily at low Mach the numerical code used against Choi et al.'s DNS. The physical size of each system of riblets was unchanged when going from Mach 0.33 to Mach 1.5. In these simulations, the "high" riblet turns out to reduce the drag ($\approx 5\%$ for the mean friction coefficient at Mach 1.5, against $\approx 3\%$ at Mach 0.33). The

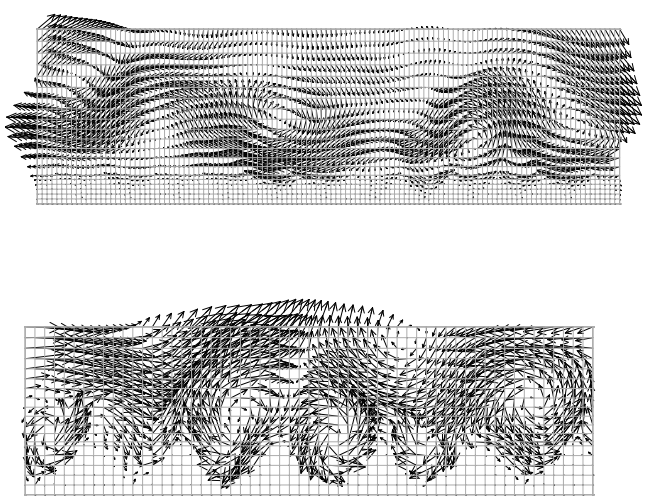

Figure 4. Cross section of the velocity in a channel above riblets at Mach 0.33; top, "high" riblet; bottom, "great" riblet (courtesy G. Hauët).

"great" one increases it. Hauët recovers the same vortex phenomenology as Choi et al. (1993), with longitudinal vortices above the riblets tips in the "high"-riblet case, and inside the valleys in the "great"-riblet case. This is confirmed by two animations which present longitudinal vorticity in Hauët's high- and great-riblet study at Mach 0.33. Figure 4 shows an instantaneous projection of the velocity vector in a cross section for the two riblets. It is clear from these animations and plots that alternate vortices lie within the valleys for the great riblet, while thinner longitudinal vortices stay above the peaks for the high riblet.

If, in a free compressible boundary layer, the optimal physical size of riblets does not vary from subsonic to supersonic regimes, then a plane will be able with the same riblets system to reduce drag at all speeds. Similar conclusions have been drawn from experiments carried out by Coustols and Cousteix (1994). This is quite satisfactory from the point of view of plane designers.

3. Some Concluding Remarks

It is now obvious from comparisons with experiments and DNS that LES are a unique tool to study both coherent-vortex dynamics and statistics in a wide class of turbulent flows. LES are faster than DNS by a factor going from approximately 10 at low Reynolds number to 100 at high Reynolds.

LES models we have used are universal in the sense that they are fixed once for all, and need no further adjustment when various external forcings or actions such as rotation, separation, thermal stratification or compressibility are considered. This makes a great difference with respect to Reynolds Averaged Navier-Stokes (RANS) models. Another interesting point is that our models are "intelligent" and adapt automatically to the flow conditions: they are inactive for laminar or transitional flows, which permits thus to study the whole transition to fully-developed turbulence. Contrary to RANS, LES give deterministic informations on high-amplitude kinematic or thermal fluctuations, which are crucial for systems safety. LES are very well adapted to simulate control systems in combustion or aeroacoustics, and see in details the effect of vortex manipulation. For more complex industrial applications, I think the next few years will see a great advance with the merging of LES and unstationary RANS which, to me, are just loosely-resolved large-eddy simulations.

References

R.A. Antonia, M. Teitel, J. Kim, and L.W.B. Browne, Low-Reynolds-number effects in a fully developed turbulent channel flow, *J. Fluid Mech.*, 236:579–605, 1992.

H. Choi, P. Moin, and J. Kim, Direct-numerical simulation of turbulent flow over riblets, *J. Fluid Mech.*, 225:503–539, 1993.

J.P. Chollet and M. Lesieur, Parameterization of small scales of three-dimensional isotropic turbulence utilizing spectral closures, *J. Atmos. Sci.*, 38:2747–2757, 1981.

G.N. Coleman, J. Kim, and R.D. Moser, A numerical study of turbulent supersonic isothermal-wall channel flow, *J. Fluid Mech.*, 305:159–183, 1995.

P. Comte, M. Lesieur, and E. Lamballais, Large and small-scale stirring of vorticity and a passive scalar in a 3D temporal mixing layer, *Phys. Fluids A*, 4:2761–2778, 1992.

E. Coustols and J. Cousteix, Performances of riblets in the supersonic regime, *AIAA Journal*, 32:431–433, 1994.

E. David, *Modélisation des Ecoulements Compressibles et Hypersoniques: une Approche Instationnaire*, PhD thesis, Grenoble University, 1993.

J.A. Domaradzki, R.W. Metcalfe, R.S. Rogallo, and J.J. Riley, Analysis of subgrid-scale eddy viscosity with the use of results from direct numerical simulations, *Phys. Rev. Lett.*, 58:547–550, 1987.

F. Ducros, P. Comte, and M. Lesieur, Large-eddy simulation of transition to turbulence in a boundary layer developing spatially over a flat plate, *J. Fluid Mech.*, 326:1–36, 1996.

M. Germano, U. Piomelli, P. Moin and W. Cabot, A dynamic subgrid-scale eddy-viscosity model, *Phys. Fluids A.*, 3:1765–1760, 1991.

D. Gottlieb and E. Turkel, Dissipative two-four methods for time-dependant problems, *Math. Comp.*, 30:703–723, 1976.

G. Hauët. *Contrôle de la Turbulence par Simulation des Grandes Echelles en Transport Supersonique*, PhD thesis, Grenoble University, 2003.

J. Hunt, A. Wray, and P. Moin, Eddies, stream, and convergence zones in turbulent flows, *Center for Turbulence Research Rep.*, CTR-S88:193, 1988.

J. Jeong and F. Hussain, On the identification of a vortex, *J. Fluid Mech.*, 285:69–94, 1995.

J. Jimenez, Turbulence, [in:] *Perspectives in Fluid Mechanics*, G.K. Batchelor, H.K. Moffatt, and M.G. Woster [Eds.] Cambridge University Press, 283–231, 2000.

R.H. Kraichnan, Eddy viscosity in two and three dimensions, *J. Atmos. Sci.*, 33:1521–1536, 1976.

E. Lamballais, O. Métais, and M. Lesieur, Spectral-dynamic model for large-eddy simulations of turbulent rotating channel flow, *Theor. Comp. Fluid Dyn.*, 12:149–177, 1998.

R. Lechner, J. Sesterhenn, and R. Friedrich, Turbulent supersonic channel flow, *J. Turbulence*, 2:001, 2001.

M. Lesieur and O. Métais, New trends in large-eddy simulations of turbulence, *Ann. Rev. Fluid Mech.*, 28:82–45, 1996.

M. Lesieur, *Turbulence in Fluids*, 3rd edition, Kluwer, 1997.

M. Lesieur, P. Begou, E. Briand, A. Danet, F. Delcayre, and J.L. Aider, Coherent-vortex dynamics in large-eddy simulations of turbulence, *Journal of Turbulence*, 4:016, 2003.

M. Lesieur, O. Métais, and P. Comte, *Large-Eddy Simulations of Turbulence*, Cambridge University Press, in press, 2004.

O. Métais and M. Lesieur, Spectral large-eddy simulations of isotropic and stably-stratified turbulence, *J. Fluid Mech.*, 239:157–194, 1992.

D. Papamoschou and A. Roshko, The compressible turbulent shear layer: an experimental study, *J. Fluid Mech.*, 197:453–477, 1988.

T. J. Poinsot and S. K. Lele, Boundary conditions for direct simulations of compressible viscous flows. *J. Comp. Phys.*, 101:104-129, 1992.

N.D. Sandham and W.C. Reynolds, Three-dimensional simulations of large eddies in the compressible mixing layer. *J. Fluid Mech.*, 224:133-158, 1991.

H. S. Sandhu and N. D. Sandham, Boundary conditions for spatially growing compressible shear layers, *Tech. rep.*, Department of Aeronautical Engineering, Queen Mary & Westfield College, 1994.

C. Silva and O. Métais, Vortex control of bifurcating jets: A numerical study, *Phys. Fluids*, 14:3798–3819, 2003.

J. Smagorinsky, General circulation experiments with the primitive equations, *Mon. Weath. Rev.*, 91-3:99–164, 1963.

A. Witkowska and D. Juvé, Estimation numérique du bruit rayonné par une turbulence homogène et isotrope, *C. R. Acad. Sci. Paris, Ser II*, 318:597–602, 1994.